ISSN: 2249-7196
IJMRR/ Oct 2021/ Volume 11/Issue 4/-/1-09
Tayfun E. Tezduyar / International Journal of Management Research & Review

Simulating fluid-structure interactions using dynamic meshes that depend on interface projection

Tayfun E. Tezduyar , Jason Crabtree, J. Crabtree
Mechanical Engineering, Rice University,
MS 321, 6100 Main Street, Houston, TX 77005, USAe-mail: tezduyar@rice.edu
Civil and Mechanical Engineering, US Military Academy,West Point, NY 10996, USA

Abstract; The Team for Advancing Flow Simulation and Modeling developed a technique called stabilized space-time fluid-structure interaction (SSTFSI), which has been used to evaluate several 3D examples such arterial fluid mechanics and parachute aerodynamics (TAFSM). We focus in this article on interface projection techniques that have evolved as complementary methods for addressing the computational challenges brought on by the geometric complexities of the fluid-structure interface. The SSTFSI approach and the study of air-fabric interactions inspired the development of these supplemental methods; nevertheless, they are relevant to other types of FSI applications and may be utilized with other moving-mesh techniques, such as the Arbitrary Lagrangian-Eulerian (ALE) technique. The FSI Geometric Smoo- thing Method (FSI-GST), Homogenized Modeling of Geometric Porosity, split nodal values for pressure at fabric edges, and incompatible meshes at air-fabric interfaces are some of the current supplemental approaches (HMGP). The model's membrane might be stabilized by using split nodal values for pressure at the edges and incompatible meshes at the interfaces, both of which would reduce the resulting structural reaction at the edges. To mitigate the impact of the structure's complex shape on the fluid mechanics mesh, the FSI-GST is implemented. By replacing the geometric permeability with a locally variable "equivalent," the HMGP avoids the difficult details of the underlying geometry.
Keywords; Space-time FSI is used for sails and parachutes, while other interface projection techniques account for air-fabric contact and fluid-structure interaction.

1 Introduction

Recent years have seen a surge in interest in simulating fluid-structure interaction (FSI) (see, for example, [1–30]). From blood circulation (11,14,17,19,26,30) to bridges (24), tents (25), pipelines (4), and parachutes (6-8, 10, 15, 16, 18), it was employed for all of these and more. Nine out of ten authors from the aforementioned research agree that the ALE finite element formulation [31] provides the best accurate results when it comes to interface tracking (moving mesh). When the structure moves, the fluid's spatial domain takes on a different shape, necessitating that the mesh itself move to accommodate this, as well as move to follow (or "track") the fluid-structure interface. Because of this, we may control the mesh resolution at the interface and get accurate solutions in these crucial flow zones by moving the fluid mesh to track the interface, at least for interfaces with manageable geometric complexity. Several of the aforementioned ALE-based FSI algorithms use the Streamline-Upwind/Petrov-Galerkin (SUPG) [32,33] and Pressure-Stabilizing/Petrov-Galerkin (PSPG) [34,35] formulations. SUPG formulation may avoid numerical instabilities while dealing with high Reynolds number and thick boundary layers. By using the PSPG formulation, we avoid numerical instability while employing equal-order interpolation functions for velocities and pressures. Pressure stabilization for Stokes flows was initially suggested in [36].
The TAFSM created the Deforming-Spatial-Domain/Stabilized Space-Time (DSD/SST) formulation [34,37,38] in 1991, and it has been utilized since since as the interface-tracking method. SUPG and PSPG are also used as stabilizing strategies in the DSD/SST formulation. More closely depicting the implementation used in those computations, the DSD/SST formulation described in [39] has been used by the TAFSM.

beginning (see Comment 1 in [40]). (see Comment 1 in [40]). (for more, see [40]'s Comment 1). As first conceived, the DSD/SST formulation envisioned a mesh update process that would include shifting the mesh over many time steps before resorting to a full remeshing. The mesh may be repositioned using the method described in [41] and expanded upon in [42]. Due in large part to the TAFSM, the generic mesh update method described in [41] has been vastly enhanced. The need for remeshing is much reduced because to these enhancements (see to [18,40,42-47]). The DSD/SST formulation and these complex mesh update techniques provide the backbone technology of the TAFSM's space-time FSI approaches. It was reported in 1992 that space-time FSI techniques were utilized to calculate 2D flows, namely the motion of a cylinder in uniform and shear flows [34,37,38] and the vibration of a cylinder generated by a vortex [48]. It was shown in [4] in 1995 that a 1D structure (a flexible cantilevered pipe) exposed to a flow may have its vibrations properly predicted using 3D flow calculation. Parachute inflation was initially described using axisymmetric FSI calculations in [49], which was published in 1997. In the context of parachutes, applications to 3D FSI computations with incompressible flows, membranes, and cables were first published in [6-8,50-53] in 1999. These preliminary applications were calculated using the block-iterative coupling approach (see [15,16,40] for the terminology and context). Newer, more refined forms of these first block-iterative approaches were developed and used to a wide range of test issues [10,15,16,54–57]. The quasi-direct [10,15,16] and direct

coupling techniques [10,15,16] offer more robust algorithms for FSI computations in which the structure is light and, hence, more sensitive to the fluctuations in the fluid dyna- mics forces.
The stabilized space-time FSI (SSTFSI) approach was recently introduced in [40]. Using the next-generation DSD/SST

formulations given in [40], it improves upon the usefulness and efficiency of the space-time FSI approaches first developed by the TAFSM. In [40] and the cited works ([58–61]), many 3D examples were used to demonstrate the applicability of the SSTFSI approach in real-world scenarios, such as arterial fluid mechanics [58,60].

Due to the geometric complexity of the interface structure, it may be essential to use a costly, unwanted, or unmanageable fluid mechanics mesh. Perhaps the most often mentioned benefit of the interface-capturing (fixed-mesh) method is this. This technique is an example of an approach to interface representation since its central tenet is that the fluid mechanics mesh does not move to follow the interfaces. Nevertheless, it is important to remember that, even with an accurately represented interface geometry, the resolution of the boundary layer will be limited by the resolution of the fluid mesh at the position of the interface when simulating fluid-structure interactions. Hence, for interfaces with sufficient geometric complexity, if a moving-mesh method can be used with an acceptable reme- shing cost, its fluid mechanics accuracy at the contact will be superior to that of a fixed-mesh approach (see [40] for different remeshing alternatives). Yet, it is vital to remember that fixed-mesh approaches become more desirable when the interface geometric complexity seems to be too high for a moving-mesh method, even if it is apparent that the two goals are not identical. Consequently, it is not hard to imagine that if we relax our expectations for good fluid mechanics accuracy near the interfaces with high geometric complexity, we can find a number of ways to make the problem computable also with moving- mesh methods, and we can still expect to obtain good accuracy near the interfaces with reasonable geometric complexity.

Here, we describe the interface projection techniques we developed to overcome the computational challenges posed by the complex geometry of the fluid-structure interface. We developed these supplementary approaches in addition to the SSTFSI technique and in the context of air-fabric interactions. Both SSTFSI-TIP1, as detailed in Comments 5 and 10 of [40], and SSTFSI-SV, as stated in Comments 6 and 10 of the same publication, are used in the computations shown here. It is assumed that the cloth is linearly elastic since the membrane element does not indicate bending stiffness. The supplementary techniques we describe here may be used in conjunction with other moving-mesh methods, such as the Arbitrary Lagrangian-Eulerian (ALE) method, where the structure to be represented is not a fabric but rather something that needs to be addressed using shell or continuum components.

To address an FSI problem including interactions between air and fabric, numerical challenges occur. Stabilizing the structural response at the margins of the membrane structures, which lack bending stiffness, is another challenge. The fluid mechanics mesh must be shielded from the effects of the structure's geometric complexity.

The fluid mechanics mesh suffers when edges flex excessively owing to a lack of bending stiffness. We utilize SSTFSI with two complimentary approaches that assist mitigate this issue. The first is the recommendation in Comment 9 of [40], whereby split nodal values are used for pressure not only inside but also at the margins of a membrane structure submerged in fluid. It increases the numerical stability of the membrane's rims. The second method, first described in [59], employs incom- patible meshes at the fluid-structure interface to localize the severe bending to tiny regions along the interface's edges. This is accomplished by fine-tuning the structural mesh close to the fluid-mesh interface rather than refining the fluid mesh at the boundaries.

Other methods, such as Homogenized Modeling of Geometric Porosity and the FSI Geometric Smoothing Method (FSI-GST), are developed to shield the fluid dynamics mesh from the consequences of the structure's geometric complexity (HMGP). In Section 2, we address updates to the FSI-GST, which was first introduced in [40]. The HMGP was created to address the complex computational requirements of the new ringsail parachutes that will be utilized by NASA's Orion spacecraft. It's all laid out in great detail in Section 3, so make sure you read it first. Our computational tests are described in detail in Section 4. In Section 5, we briefly recap our modeling strategy and some of our computed conclusions for the ringsail parachutist aboard the Orion spacecraft. The concluding remarks are presented in Section 6.

2 FSI geometric smoothing technique (FSI–GST)

The FSI-GST was suggested by [40] for use in simulations when a costly, unfavorable, or hard-to-control fluid mechanics mesh is required due to the geometric complexity of the structure. The displacement rates at the interface and the structural mesh are projected onto the fluid mesh after a geometric smoothing step. In geometric smoothing, a node's value (mesh coordinate or displacement rate) is replaced by a weighted average of the values at the node and a few nearby nodes. Projecting the stress values from the interface to the structure is as simple as transferring the values from the smoothed interface to the proper nodes of the structure. Unlike an isotropic geo- metric smoothing, a directed smoothing in a particular direction may be necessary for certain computations. In order to do such computations, the FSI Directional Geometric Smoo- thing Technique (FSI-DGST) was developed and originally described in [40]. The FSI-DGST, when practical, produces an interface mesh where the gridlines roughly mirror the chosen smoothing directions. If a node is on a gridline, then only nodes on the same gridline may be utilized as weights in an average. The directional smoothing notion is similar to the directional "upwind" idea since in the SUPG formulation, the residual-based numerical dissipation is only active in the streamline direction.

The radial direction of smoothing is used in the parachutist-specific variation of the FSI-DGST reported in [61,62]. The "peaks" and "valleys" of the parachute gores are formed by inflating a canopy with embedded reinforcing wires positioned longitudinally in the canopy structure, adding geometric intricacy. This FSI-DGST for parachutes generates the set of fluid interface nodes by randomly picking nodes from the structural interface mesh. As there is less need for support at fluid interfaces, there are fewer nodes there. In compiling the set of fluid interface nodes, we choose the structural interface nodes in the valleys. Choose these nodes radially to bypass certain valleys, or choose them axially to bypass specific nodes inside a valley. Following that, a fluid mesh with a smooth radial gradient is generated by connecting the nodes with triangular elements with three nodes. This analysis estimates that the

ringsail parachute has 80 gores, yet the distance the gores bulge out is little compared to the parachute's diameter. We find that precise shapes of the gores are not important for predicting the fluid dynamic forces in this class of applications. Each value (mesh coordinate or displacement rate) at any given node of the fluid interface is replaced by its equivalent value at the node of the mapping structure. The stressed interface is sent to the structure in two ways: directly for the mapping nodes, and as a weighted average for the remaining nodes. As an alternative to using the transfer rule, we suggest projecting the stresses from the fluid interface mesh to the structure interface mesh by merging the pressure and viscous components of the stress vector at the nodes of the structure interface. From this point, we'll call it the "Separated Stress Projection" (SSP). The SSP provides a more reliable projection when the fluid mechanics mesh at the interface is much coarser than the structural mecha- nics mesh and the structure interface is not sufficiently smooth at the fluid mechanics mesh size. We provide a revised version of the SSTFSI approach given in Sect. 3.3 of [40] to take into account this change in the stress projection.

3 Homogenized modeling of geometric porosity(HMGP)

An original description of the HMGP was presented in a conference article [61], where it was proposed as a solution to one of the computational challenges inherent in the FSI modeling of the new parachutes for use with NASA's Orion space spacecraft. Because of the many "rings" and "sails" used to construct a parachute's canopy, the structure has a geome- tric porosity that creates its own set of challenges. The STTFSI algorithms developed in [40] account for the realistic fabric porosity encountered during the descent of a T-10 parachute (see Eq. (28) in [40]). The HMGP approximation uses a porosity that fluctuates locally rather than globally to get past the intractable complexity of the geometric porosity. Fluid dynamics simulations show a "solid" parachute, with fabric filling the voids between the rings and sails. The structural mechanics analyses maintain the parachute canopy's distinctive rings and sails design. Fabric porosity is created to vary regionally to trick fluid mechanics calculations into thinking the solid parachute looks more like the parachute with slits. An equivalent fabric-porosity coefficient may be computed from the anticipated pressure differentials and flow rates over the parachute's canopy when geometric porosity is considered. For this, it is sufficient to do a one-time calculation of airflow through the parachutist's geometrically porous parachute. By doing so, we may ascertain a localized variation in the porosity coefficient, or in certain cases, a globally constant porosity coefficient. At first, we calculate the locally-varying porosity coefficient, and then we calibrate it by changing its size in order to get the measured resistance. In our parachute calculations, we combine the FSI-DGST and HMGP processes into a single phase, as detailed in Sections 5.2 and 5.3.
First Remark To preserve the integrity of the fluid mechanics mesh between the structural surfaces, the Surface-Edge-Node Contact Tracking (SENCT) method was recently presented as a contact algorithm (see [40]). When it was first conceived, the goal of this technology, which is still in its infancy but is undergoing extensive testing and improvement, was to prevent the fundamental

4 Test computations

The calculations detailed here are performed in a parallel computing setting, employing clusters of personal computers. Each mesh is created on a separate node inside the cluster. No remeshing was necessary for the completion of all calculations. By using the quasi-direct coupling method, the fully discretized, coupled fluid and structural mechanics and mesh-moving equations were solved in each instance (see Sect. 5.2 in [40]). Nonlinear iterations were solved by using the GMRES search algorithm [63] with a diagonal preconditioner to solve the underlying systems of linear equations.

4.1 Windsock

In [40], we saw this testing calculation described. We provide a comprehensive overview of the testing outcomes for interface projection methods. A wind-sock at the Albuquerque airport is seen in Figure 1. Our computational windsock model is 1.5 meters long, with a diameter varying from 0.25 meters in the upstream direction to 0.15 meters in the downstream direction (see Fig. 2). Initial conditions for the flow field are the produced flow field corresponding to a rigid windsock kept in the horizontal position. After that, the windsock's gravity is activated, the FSI begins, and the windsock begins to droop. The speed of the wind has always been steady at 10 meters per second. A value of 1.2 kg/m3 is applied to the air density, and a value of 1.5 x 105 m2/s is applied to the kinematic viscosity. The windsock has dimensions of 2.0 mm thickness, 100 kg/m3 density, 1.0 106 N/m2 stiffness, and 0.45 Poisson's ratio. Yet, the rest of the structure is unrestrained and flaps cyclically, while the upstream edge is locked in place. The windsock has a semi-structured mesh with 984 nodes and 1,920 triangular membrane components, each with three nodes. There are 113,245 tetrahedral elements with four nodes, and there are a total of 19,579 nodes in the fluid mechanics mesh. At first, the interface fluid mesh is the same as the windsock mesh. SSTFSI-SV is used for the computation (for more information,

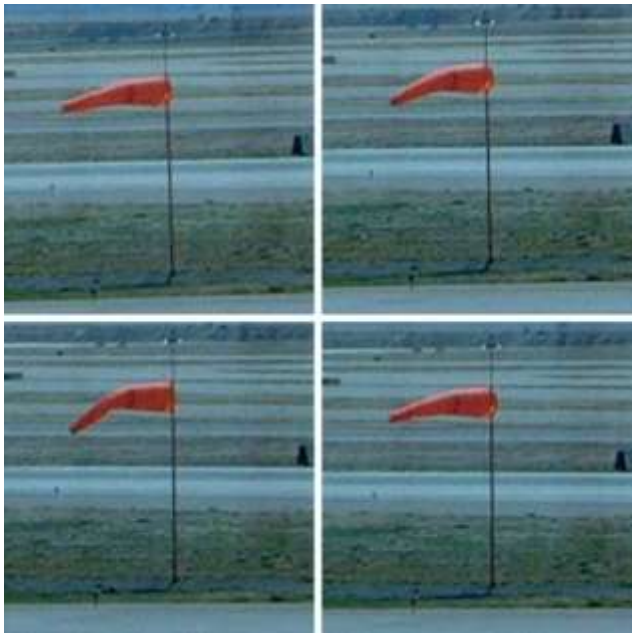

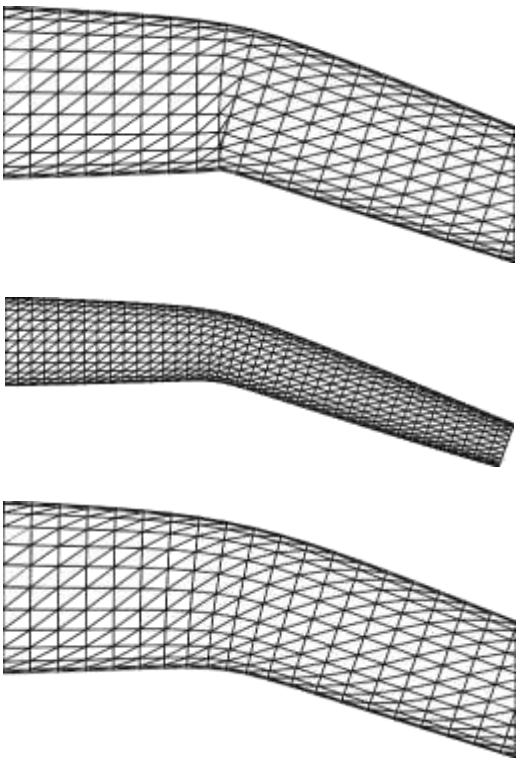

Fig. 1 A windsock. Sequence: *left to right, top to bottom*

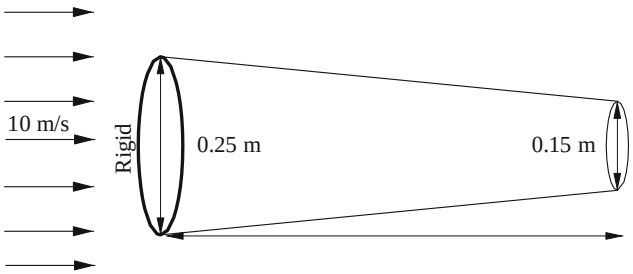

Fig. 2 Windsock. Problem setup

4.2 Sails

First described in a conference article [59], this testing technique has now been widely used. Figure 5 depicts the configuration with two sails. The mainsail's geometry and fundamental shape are inspired by plate airfoil designs, in particular those with the maximum camber of 15% cord length located at 30% cord. Comparable to the Adventuress' mainsail [64] in general shape and size. The height of the mast is 15 meters, while the width of the base is 5 meters. The nodes are only attached to the luff and foot of the mainsail, leaving the remainder of the sail free. Using a proportionate method, the same picture was utilized to create a single jib sail. A jib with a luff of 12.70 meters in length. Just the head, tack, and clew of the jib are fastened to the wires in any permanent fashion. The air is travelling at 7.72 m/s at an azimuth of 35 degrees from the horizontal (about 10 knots).

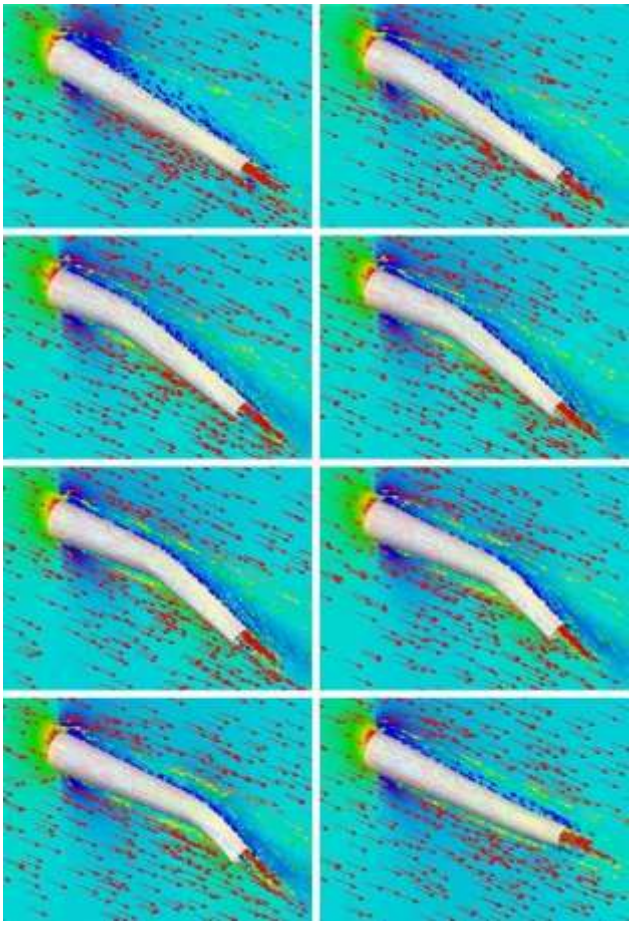

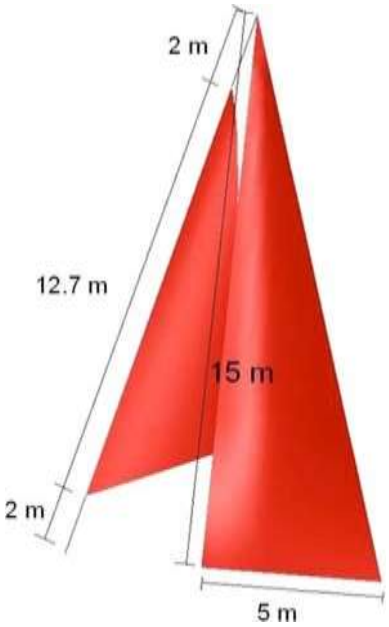

Fig. 4 The windsock and the flow field (velocity and pressure) at various instants. Velocity vectors colored by magnitude

5 a line running down the middle of the boat representing the longitudinal axis (not modeled). The kinematic viscosity of air is 1.5 x 105 m2/s, and its density is 1.2 kg/m3. Sails are 1 mm thick, weigh 1,370 kg/m3, are strong enough to withstand a force of 3.0 109 N/m2, and have a Poisson's ratio of 0.3. A diameter of 6.35 mm, a density of 1,440 kg/m3, a stiffness of 3.0 109 N/m2, and a Poisson's ratio of 0.3 characterize the cables. The fluid mechanics interface mesh and the sail meshes are shown in Figure 6. There are 654 vertices in the mainsail mesh and 1,177 MMEs (3-vertex triangles) in total. The jib sail's mesh consists of 349 nodes and 601 components. There are three different cable parts, and each one connects to two nodes, making up the cable mesh. The fluid-structure interface has 558 nodes and 952 triangular faces, whereas the fluid-mechanics mesh has 91,512 nodes and 553,183 four-node tetrahedral components. The answer is computed by using the SSTFSI-TIP1 technique (for details, see Notes 5 and 10 in [40]) and the SUPG test function option WTSA (see Remark 2 in [40]). By removing the SUGN2 term from Eq. (14), we may use Eqs (12). (14). The time-step size starts off at 0.002 s and increases to 0.004 s, 0.008 s, then 0.016 s as the algorithm continues. Iterations of a nonlinear algorithm

6 Ringsail parachute

6.1 Parachute components

Unlike the T-10, G-11, and G-12, which are all one continuous piece of fabric, ringsail parachutes are made up of many rings or sails and have an unstressed ogival form. Here, we take a look at a ringsail parachute with a profile that's a quarter of a sphere.

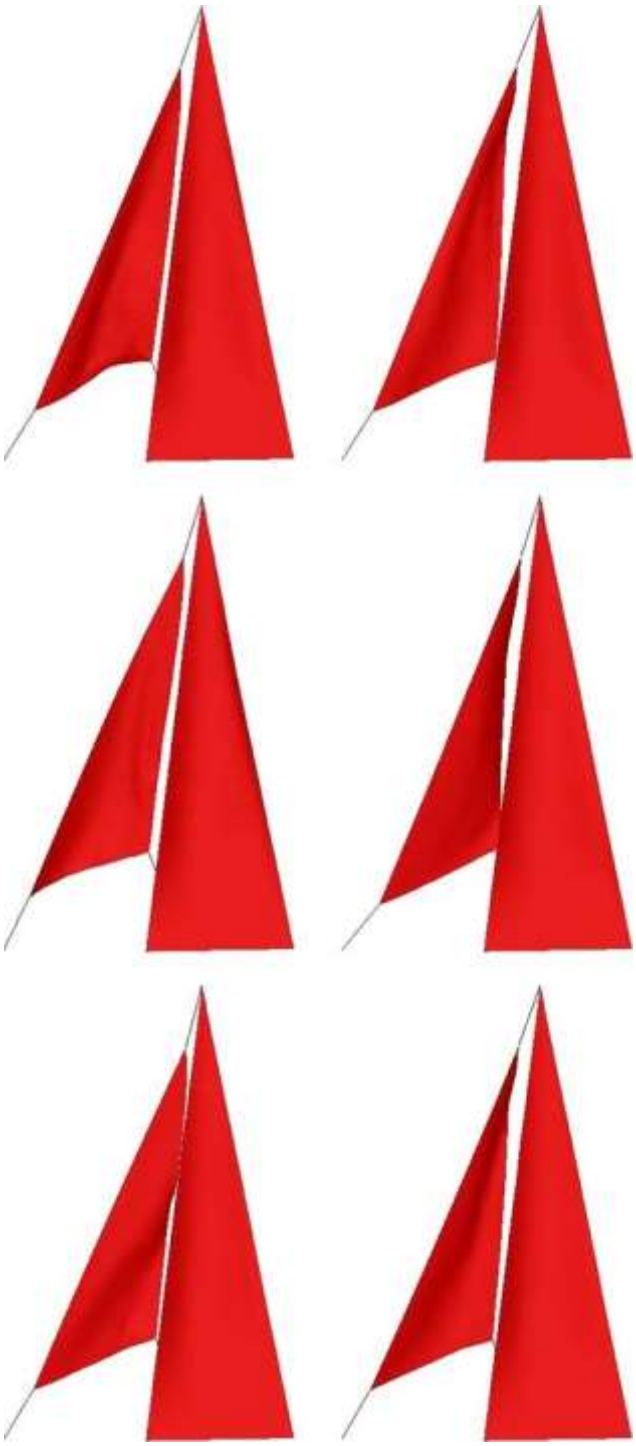

Fig. 7 Sails at various instants

in its unstressed shape. The crown portion of the ringsail parachute (the portion near the vent) is made of rings with gaps between the consecutive rings (see Fig. 8).

The middle and skirt portions of the parachute are made of sails. Two edges of the sails are stitched to the radial lines and the other two edges are free. The edge facing the parachute

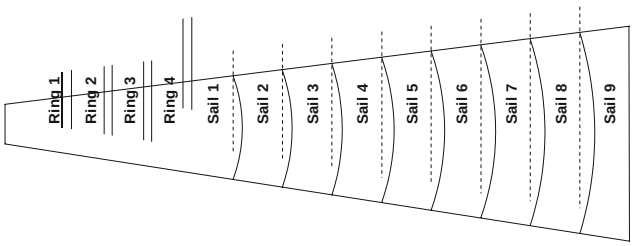

Fig. 8 Gore layout of the ringsail parachute (not drawn to scale)

The edge facing the vent is the trailing edge and the edge facing the skirt is the leading edge. It's possible for there to be fullnesses at both the leading and trailing edges, giving the appearance of bulging out even when not under stress. A sail's leading edge and trailing edge always meet at right angles. Several bands, lines, and tapes are used in the canopy's construction to provide the parachute its necessary rigidity. For instance, the development of the parachute's gores is due to the radial lines, which also offer longitudinal rigidity..

6.2 Smoothing

We do this by using incompatible meshes at the fluid-structure interface. Each ring, sail, and gore of the parachute are modeled using a fine-grained structural mesh. To pinpoint where the tension is most concentrated, a suitable mesh is required. At the interface, the fluid mechanics mesh is coarser. While creating and updating the fluid mesh at the interface, we use the FSI-GST described in Sect. 2. Hence, in the circumferential direction, we may choose every other valley node for the rings and every valley node for the sails. Each ring and sail may have any of many distinct numbers of valley nodes in the longitudinal direction, depending on where they are located..

6.3 Homogenization

Two homogenized models for geometric porosity are used. To simplify the fluid mechanics calculations, the geometric porosity of the first model is assumed to be a constant throughout the whole canopy in the second. The second model incorporates a fabric porosity that varies in different locations to stand in for the geometric porosity. Using a concentric patch method, we determine a fabric-porosity coefficient for each section of the canopy. One can see a slit in the middle of each patch, with a piece of a ring or sail on each side. Each area is assigned a porosity coefficient, and then at the boundary between two areas, the average of the two porosity coefficients is utilized. We do a one-time flow calculation, keeping the canopy rigid and utilizing a tiny slice of the canopy with a limited number of gores, with all the rings, sails, and struts in place, to determine the porosity coefficient for each patch.

6.4 Example

Our modeling of the parachutes for NASA's Orion space spacecraft is used as an example of FSI modeling of ringsail parachutes, and we provide here a very tiny fraction of the calculated findings. Parachute simulation reveals outcomes after dropping the heat shield, which accounts for around 13.5 percent of the vehicle's total mass. We think about using a single primary parachute that has to carry a third of the vehicle's mass. Figure 9 depicts the surrounding flow before and about 6 seconds after the heat shield is lowered from the parachutist's aircraft. Read [65], which not only describes this simulation in depth but also provides numerous more examples of simulations for ringsail parachutes..

7 Concluding remarks

We describe the interface projection techniques we developed to address the computational challenges brought on by the complex geometry of fluid-structure interfaces. These auxiliary methods were created in tandem with the SSTFSI technique

to account for air-fabric interactions when the fabric is represented by the membrane element, which does not provide bending stiffness. These methods may be used to a wide variety of FSI use cases, and although they are most often associated with the ALE approach, they can be used in tandem with any moving-mesh technique.

general. If the fabric has low bending stiffness, it may pucker excessively at the edges, which is problematic for the fluid mechanics mesh. We developed two complementary approaches to deal with this problem. The first is employing split nodal values to take into consideration pressure on both the inside and outside of a submerged mem- brane structure. In doing so, we improve the numerical stability of the membrane's rims. The second method uses incompatible meshes at the interface between the fluid and the structure to contain the excessive ben- ding to small regions at the borders. This is accomplished by refining the structural mesh close to the fluid mesh rather than refining the fluid mesh to the same degree at the edges. As a result of the complexity of the geometry, a fluid mechanics mesh may be required for the structure's movement, but this mesh may be excessively costly, impractical, or difficult to manage. These two supplemental approaches are computationally sound solutions to this issue. They are a kind of the FSI Geometric Smoothing Technique.
(Homogenized Modeling of Geometric Porosity) and (Finite-Scale Inhomogeneous Geometric Structure Theory) (HMGP). Both the standard FSI-GST and the parachutist-specific variation smooth the transition between the structural mesh and the fluid mechanics component in a direction-dependent manner. The fluid mechanics part of the FSI problem is protected against "irresolvable" forms of structural deformation by using this path. The HMPG was used to simulate the geometric porosity of the Orion spacecraft's raingsail parachutes. Canopy geometric porosity is a result of the many "rings" and "sails" that make up its structure. The HMGP sidesteps this intractable complexity by approximating the geometric porosity with a fabric porosity that varies over its surface. Using a windsock, a sailboat, and a paraglider equipped with a raingsail as numerical examples, we show how to compute air-fabric interactions. Our results demonstrate that the SSTFSI approach, together with the supplementary methodologies we provided, may be used to solve the computational issues brought on by the geometric complexity of the fluid-structure interface.

Acknowledgments This work was supported in part by NASA Johnson Space Center under Grant NNJ06HG84G. It was also suppor- ted in part by the Rice Computational Research Cluster funded by NSFunder Grant CNS-0421109, and a partnership between Rice University, AMD and Cray.

References

1. 1 Tezduyar, Aliabadi, Behr, Johnson, and Mittal (1993) Parallel finite-element computation of three-dimensional flows. Number Theory 26:27-36
2. Tezduyar TE, Aliabadi SK, Behr M, and Mittal S., "Massively parallel finite element modeling of compressible and incompress- ible flows" (1994). To be published in Comput. Methods. Appl. Mech. Eng. 119:157-177.
3. Computation of incompressible flows with fluid-body interactions using massively parallel finite elements. Mathematical and Computational Methods in Applied Mechanics and Engineering 112:253-282, 1994, S. Mittal and T. E. Tezduyar.
4.
5. Multi-core parallel finite element analysis of incompressible three-dimensional flows with structure-fluid interactions. Journal of Information and Computational Methods in Fluids, 21(9), 933-953.
6. 5. Enhanced methods for creating and updating meshes for 3D flow simulations. Tezduyar TE, Johnson AA (1999). Computer Mechanics, 130–143.
7. Tezduyar TE, 6-Kalro V (2000) Simulation of fluid-structure interaction in three-dimensional parachute systems using parallel computing. Reference: Computerized Techniques. Mechanical Engineering, 190:321–332
8. 7. 7 Katherine Stein; Robert Benney; Vladimir Kalro; Theodore Tezduyar; Joseph Leonard; Maria Accorsi (2000) Parachutist parachute CFD simulation. Applications of Computational Methods in Engineering and Mechanics 190:373–386
9. 8 The effects of the plane's distant wake on the parachutes' fluid-structure interactions, Tong Tezduyar and Yukio Osawa (2001). Find it in issues 717-726 of volume 191 of the journal Comput Methods in Applied Mechanics and Engineering.
10. Internal structural acoustic and hydroelastic sloshing systems: simplified symmetric models for modal analysis 9 (Ohayon, R., 2001). 190:3009-3019 Computerized Techniques. Applied Mechanics and Engineering.
11. Ten. Space-time methods for finite element computation of flows with fluctuating bou- daries and interfaces. TE Tezduyar, S. Sathe, R. Keedy, and K. Stein (2004). Gallegos, Herrera, Botello, Zarate, and Ayala, editors, Proceedings of the Third International Conference on Numerical Methods in Engineering and Applied Science, CD-ROM, Monterrey, Mexico.
12. Torii R, Oshima M, Kobayashi T, Takagi K, and Tezduyar TE (2004) published in Jpn Soc Mech. Eng. Journal Part A 70:1224-1231, "Image-based blood flow modeling with the influence of wall elasticity."
13. An article on the nonnormality of subiteration was written by van Brummelen and de Borst in 2005 for a special issue on fluid-structure interaction. SIAM Journal of Scientific Computing, Volume 27, Pages 599-621.
14. 13. Thirteen. C. Michler; E. H. van Brummelen; R. de Borst (2005) A fluid-structure interaction interface for the Newton-Krylov solver. A Publication of the International Association for Numerical Methods Fluids 47(9):1189-1195
15. 14 Gerbeau, Jean-François, Mihail Vidrascu, and Paul Frey. 2005. Fluid-structure interaction in blood flow geometries based on medical images. The Journal of Computational Structures 83:155-165
16. 15 Fluid-structure interaction computation using space-time finite element methods. 2006 Tezduyar TE, Sathe S, Keedy R, Stein K. 195:2002-2027 in Comput. Methods. Appl. Mech. Eng.
17. Tezduyar TE, Sathe S, and Stein K (2006) in Comput. Methods. Appl. Mech. Eng. 195:5743-5753 propose solution techniques for the fully-discretized equations involved in calculating fluid-structure interactions utilizing space-time formulations.
18. Formulation using deforming spatial domains and stabilized space-time for Researchers: Torii, R., Oshima, M., T. Kobayashi, K. Takagi, and

T.E. Tezduyar (2006)

19.

20. simulated the fluid-structure interactions in the heart and blood vessels. 195:1885-1895 in the journal Comput. Methods. Appl. Mech. Eng.
21. 18.
22. Space-time modeling of fluid-structure interactions. On pages 50-81 of Volume 53 of Lec- ture Notes in Computational Science and Engineering, Springer, Heidelberg, 2005, edited by H.-J. Bungartz and M. Schafer, you'll find work by Tezduyar TE, Sathe S, Stein K, and Aureli L. Analyzing the effects of hypertension and normal blood pressure on the fluid-structure interaction of aneurysms. Twenty-First Century Physics 38:489-490 (2006) Torii R, Oshima M, Kobayashi T, Takagi K, Tezduyar TE Mechanical and Computer Engineering. Authors: W. Dettmer & D. Peric (2006) As a computational starting point, this area of research might look to the finite element technique and its uses in the field of fluid-structure interaction. Information Processing Methods 195:5754-5779 21.Appl. Mech. Eng. Yakov Bazilevs, Vladimir M. Calo, Yue Zhang, and Timothy J. R. Hughes conducted an isogeometric investigation of fluid-structure interactions with arterial blood flow applications. 2006. Computer Mechanics 38:310-322 22. Multiscale/stabilized formulation of the incompressible Navier-Stokes equations for fluid-structure interaction and moving-boundary flows by Khurram RA and Masud A. (2006). Mech. 38:403-416 (Comput.), (Comput.), 23. With the use of pure Dirichlet fluid domains, Kuttler U, Forster C, and Wall WA (2006) found a way to solve the incompressibility issue in fluid-structure interaction (38:417-429). 24 Computer and Mechanical Engineering. Making the loose coupling method more usable in FSI simulations. Drs. Lohner, Cebral, Yang, Baum, Mestreau, Soto, and Soto (2006). Edited by H.-J. Bungartz and M.-P. Schafer, "Fluid-structure Interaction" is volume 53 of Lecture Notes in Computational Science and Engineering. Refer to Springer, Heidelberg, pages 82–100.
23. Kristina-Utah Bletzinger, Robert Wuchner, Adam Kupzok, and (2006) An algorithmic analysis of shells and free-form membranes in FSI. H.-J. Bungartz and Michael Schafer, eds., Lecture Notes in Computational Science and Engineering, Volume 53. 20 A. Springer, Heidelberg, pages 336–355. T. E. Tezduyar, R. Torii, M. Oshima, T. Kobayashi, K. Takagi, and R. Torii (2007) The effects of wall elasticity are investigated in patient-specific hemody- namic models. 36:160-168 Computational Fluid Dynamics